DOI https: //doi. org/10.1007/s11595-018-1953-2

Effects of Aging Treatment on Intergranular Corrosion and Stress Corrosion Cracking Behavior of AA7003

ZHANG Xiaoyan[1,2,3], SONG Renguo[1,2,3*], SUN Bin[1,2,3]

(1. School of Materials Science and Engineering, Changzhou University, Changzhou 213164, China; 2. Jiangsu Key Laboratory of Materials Surface Science and Technology, Changzhou University, Changzhou 213164, China; 3. Jiangsu Collaborative Innovation Center of Photovolatic Science and Engineering, Changzhou University, Changzhou 213164, China)

Abstract: In order to study the effects of aging treatment on the intergranular corrosion (IGC) and stress corrosion cracking (SCC) of 7003 aluminum alloy (AA7003), the intergranular corrosion test, electrochemical test and slow strain rate test (SSRT), combined with optical microscopy (OM) and scanning electron microscopy (SEM) as well as transmission electron microscopy (TEM) observations have been carried out. The IGC and electrochemical test results showed that the IGC resistance of AA7003 for peak aged (PA) temper is the lowest, with double peak aged (DPA) the moderate, and retrogression and re-aging (RRA) the highest among three tempers, which is attributed to the continuous feature of precipitation on grain boundary of PA temper and the interrupted feature of precipitation on grain boundary of DPA and RRA tempers, as well as the wide precipitation free zones (PFZ) of RRA temper. In addition, the SSRT results indicated that all three tempers AA7003 are susceptible to SCC in IGC solution, and the change tendency of SCC susceptibility (I_{SCC}) of AA7003 for three tempers follows the order: I_{SCC}(RRA)<I_{SCC}(DPA)<I_{SCC}(PA).

Key words: AA7003; aging treatment; intergranular corrosion; stress corrosion cracking

1 Introduction

7003 aluminum alloy (AA7003) belongs to 7000 series (Al-Zn-Mg-Cu) aluminum alloys which have preeminent combination of properties such as fracture toughness, high specific and thermal conductivity[1-4]. These superior properties result in a considerable amount of studies devoted to developing aluminum alloys used as structural materials in aircraft, space vehicles, and automotive applications in the past several decades[5-9].

Corrosion is one of the main failure forms of aluminum alloys, and Al–Zn–Mg–Cu alloys are strongly susceptible to the localized corrosion[10,11], such as pitting, intergranular corrosion (IGC), stress corrosion cracking (SCC) and so on. The poor corrosion resistance limits the applications of Al–Zn–Mg–Cu alloys[12-16]. In the past several decades, some investigations have been carried out to study the relationships between the heat treatment, microstructural evolution and properties of Al-Zn-Mg-Cu alloys[17–22]. Rout *et al*[11] studied the influence of aging treatment on SCC behavior of Al-Zn-Mg-Cu alloy and found that 7000 series aluminum alloys have the highest strength in their peak-aged (PA) temper, but they are more susceptible to localized corrosions. However, Angappan and Han *et al*[17,18] found that the retrogression and re-aging (RRA) provides an optimum combination of the fracture toughness and strength during the study of the effects of pre-stretching and aging on the microstructure, strength and fracture toughness of 7050 aluminum alloy. In addition, Xiao *et al*[19] reported that RRA can increase the size and distribution discontinuity of grain boundary precipitates and lead to the increase of the corrosion resistance without the loss of strength and ductility of an Al-Zn-Mg-Cu alloy. In order to spread the use of 7000 series aluminum alloys in industries, it is still of great significance to investigate the effects of aging treatment on localized corrosion behaviors such as IGC and SCC of aluminum alloys.

Aging treatment is the key process to achieve the excellent associated properties. The decomposition of super saturation solid solution (SSSS) during the aging contributes to the formation of some second

(Received: May 18, 2016; Accepted: June 21, 2018)

ZHANG Xiaoyan (张晓燕): Postgraduate; E-mail: 1134514866@qq.com

*Corresponding author: SONG Renguo (宋仁国): Prof.; Ph D; E-mail: songrg@cczu.edu.cn

Funded by the National Natural Science Foundation of China (No. 51371039)

phase precipitates in Al-Zn-Mg-Cu alloys. Usually, the precipitation sequence can be represented as follows: [23-25]

Super saturation solid solution (SSSS)→GP zones→semi-coherent $\eta'(MgZn_2)$→incoherent η ($MgZn_2$).

The aim of the present study was to determine the respective roles of aging treatment systematically during the whole corrosion process of AA7003 in IGC solution. Furthermore, the effects of aging treatment on the IGC and SCC behaviors of AA7003 were investigated by electrochemical testing, IGC testing, slow strain rate test (SSRT), and optical microscopy (OM). The microstructure of the grain boundaries was observed by transmission electron microscopy (TEM) and the fracture morphology was observed by scanning election microscopy (SEM).

2 Experimental

The AA7003 used in the present study was supplied by Alcoa Co. in the form of smooth specimens machined from a 40 mm thick rolled plate. The chemical composition (wt%) of the AA7003 is given in Table 1. The detailed conditions for the heat treatment are listed in Table 2.

Table 1 Chemical composition of AA7003/wt%

Zn	Mg	Cu	Zr	Ti	Mn	Cr	Fe	Si	Al
0.6	0.6	0.2	0.1	0.2	0.3	0.2	0.35	0.3	Bal.

Table 2 The heat treatment parameters of AA7003

Aging	Parameters
Peak aged (PA)	470 ℃×2 h+120 ℃×50 h
Double peak aged (DPA)	470 ℃×2 h+120 ℃×120 h
Retrogression and re-aging (RRA)	470 ℃×2 h+120 ℃×48 h+ 205 ℃×10 min+120 ℃×48 h

The IGC tests were performed according to ASTM G110 [26]. The solution temperature was maintained at 35±2 ℃ by a thermostat. The surface area and the solution volume ratio was 6 mm^2/mL.

The electrochemical experiments were conducted in a local electrochemical cell, using the standard three electrodes configuration: saturated calomel electrode (SCE) as a reference, a platinum plate as the counter electrode and the specimen as the working electrode. The specimens used for the electrochemical tests were mounted with epoxy resin to provide an exposed area of 1 cm^2 and was polished by successive silicon carbide paper up to 1000 #. The specimens were then rinsed with deionized water, degreased in acetone and dehydrated ethanol by ultrasonic sound, and dried in air. Potentiodynamic polarization tests were performed at a scan rate of 1 mV/s in IGC solution. The potential ranged from −1.4 V *vs* SCE to −0.3 V *vs* SCE. The potentiodynamic curves were fitted using Corrview software in the mode of Tafel (Traditional). Electrochemical impedance spectroscopy (EIS) tests were conducted at open circuit potential (OCP) after immersing in solutions for a few minutes. The EIS was obtained in the frequency range from 100 kHz to 0.04 Hz with ten points per decade and a perturbation amplitude of 10 mV. The impedance data were interpreted on the basis of equivalent electrical circuits using the Zsimpwin program for fitting the experimental data.

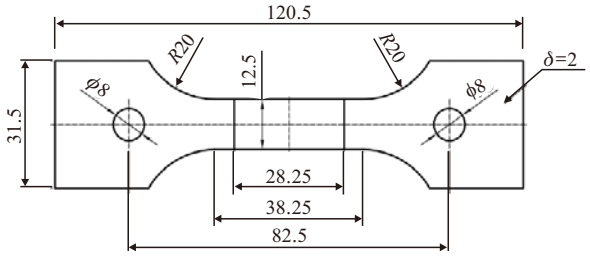

Fig.1 Schematic diagram of the SSRT specimen

Slow strain rate test (SSRT) was carried out with a strain rate of 9.5×10^{-7}/s to evaluate the SCC behavior in IGC solution. The tensile specimens were machined into smooth flat-plate specimens (see Fig.1). The specimens were ground sequentially with 1500 # grit emery papers in a grinding direction parallel to the loading direction before each SCC test. The specimens were then rinsed with deionized water, degreased in dehydrated ethanol and acetone by ultrasonic cleaner, and sealed with epoxy resin, except for the gauge sections. In addition, the tensile specimen was then applied a pre-loading force of approximately 200 N to avoid the gap between the specimen and SSRT machine. The SCC susceptibility (I_{SCC}) is defined as follows:

$$I_{SCC}=1-\varepsilon_{SCC}/\varepsilon_0 \quad (1)$$

where I_{SCC} is the whole SCC susceptibility of alloy, ε_{SCC} is the elongation to fracture in corrosive environment, and ε_0 is the elongation in dry air. I_{SCC} reflects the extent of SCC susceptibility, the higher the I_{SCC} value, the higher the susceptibility to SCC. To ensure the accuracy of the test, three samples were tested for the

average value. The standard deviation was within 5%.

The lengthwise section of the IGC sample was observed by OM. The microstructure of AA7003 was observed by means of a TEM (JEOL 2100) and the specimens were prepared by the standard twin-jet electropolishing method using 75% methanol and 25% nitric acid solution at 30 ℃. The fracture morphology of AA7003 was investigated by means of SEM (JSM-6510 and SUPRA55).

3 Results and discussion

3.1 IGC behavior

Fig.2 shows the optical morphologies of AA7003 under various tempers immersed in IGC solution for 12 h. It can be seen that all the samples under various tempers were evidently damaged by IGC to some extent. The corrosion degree could be described by maximum corrosion depth and global corrosion condition. The maximum corrosion depths of AA7003 with temper of PA and DPA are about 83 and 55 μm respectively, and the IGC levels of both tempers are 3; while the maximum corrosion depth of RRA is 10 μm and its IGC level is 1. Also, the corrosion form of AA7003 of RRA (Fig.2(c)) has transformed from IGC to uniform corrosion. Therefore, the results show that the IGC resistance of AA7003 under various tempers follows the order: PA<DPA<RRA, which may result from the difference of precipitates distribution on the grain boundaries.

3.2 Electrochemical analysis

Table 3 Electrochemical data of AA7003 under various tempers in IGC solution

Aging	E_{corr}/V	I_{corr}/(mA·cm^{-2})	b_a/V	b_c/V	R_p/(Ω·cm^2)
PA	−0.821 77	3.1	0.142 03	8.745 7	19.363
DPA	−0.807 31	1.2	0.114 31	76.137	39.783
RRA	−0.812 98	0.3	0.086 127	551.03	117.43

The potentiodynamic polarization curves in IGC solution for the PA, DPA and RRA tempers of AA7003 are shown in Fig.3. It can be seen that the corrosion potentials (E_{corr}) of AA7003 under various tempers are almost the same in IGC solution. Moreover, the anodic branch of the polarization curves exhibits typical active metal dissolution behavior since the current density increases sharply with increasing anodic potential, and the localized corrosion will occur when the potential surpasses E_{corr}. Table 3 presents the electrochemical data such as corrosion potential (E_{corr}), corrosion current density (i_{corr}) and the cathodic and anodic Tafel slopes (b_a, b_c) obtained from the polarization curves. Furthermore, the value of R_p was calculated by the stern formula:

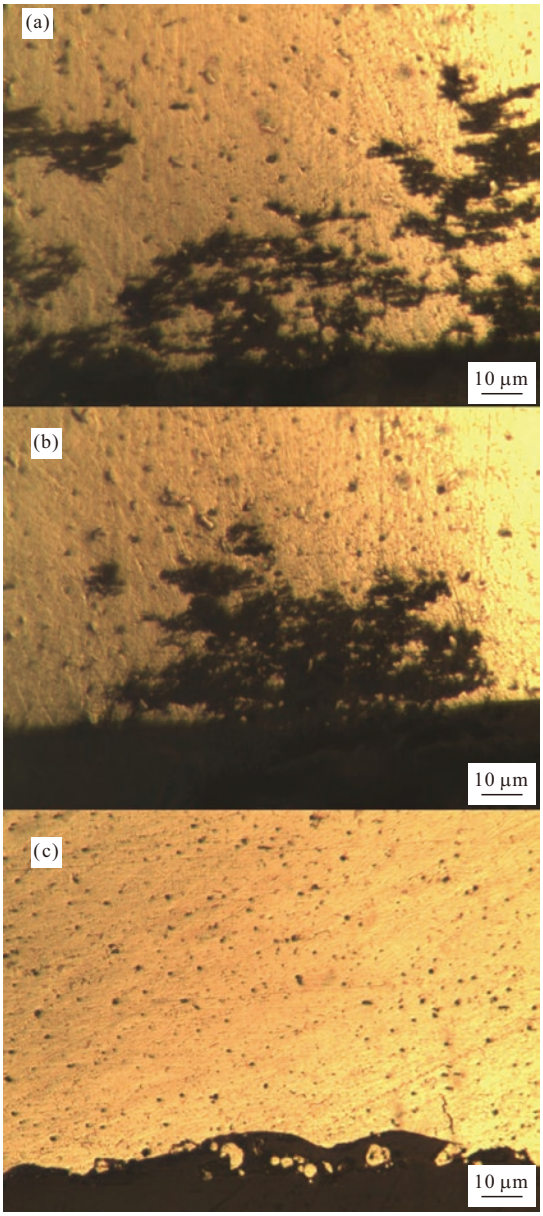

Fig.2 Optical morphologies of AA7003 under various tempers after immersed in IGC solution for 12 h: (a) PA; (b) DPA; (c) RRA

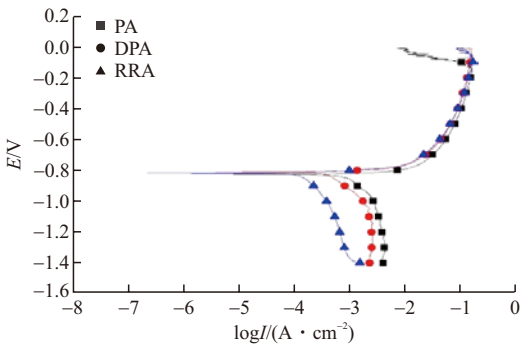

Fig.3 Potentiodynamic polarization curves of AA7003 under various tempers in IGC solution

$$R_p=b_a\times b_c/(2.3(b_a+b_c)\times I_{corr}) \quad (2)$$

The fitting results indicated that i_{corr} value of AA7003 under the temper of PA is the highest, that of DPA is moderate , and that of RRA is the least. Besides, the R_p value of PA tempered AA7003 is the lowest, and RRA the highest. Therefore, the corrosion resistances of three tempers show the following order: RRA>DPA>PA. This result is in good agreement with the result of the IGC tests.

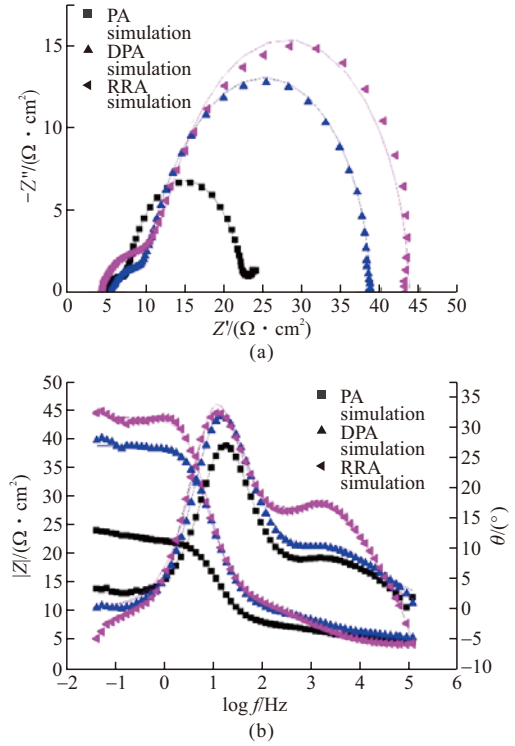

Fig.4 Nyquist (a) and Bode (b) plots of EIS of AA7003 under various tempers in IGC solution.

EIS tests were performed under open circuit potential to investigate the electrode reaction process of AA7003 under various tempers exposed in IGC solution. Fig.4 shows the Nyquist and Bode plots of the EIS. As shown in Fig.4 (a), two capacitance loops exist in the Nyquist plots, indicating that two time constants are present in EIS. In addition, there exist two remarkable peak values in the curves of phase angle in the Bode plots, which also implies that two time constants are present in EIS. Furthermore, it can be seen from the Nyquist plots that the diameters of the capacitance loops under various aging treatment are different. Specifically, the diameter of RRA is larger than that of DPA and PA, and the diameter of PA is the smallest. According to the Bode plot of |Z| *vs* frequency, it is found that the values of |Z| also comply with the order: PA<DPA<RRA.

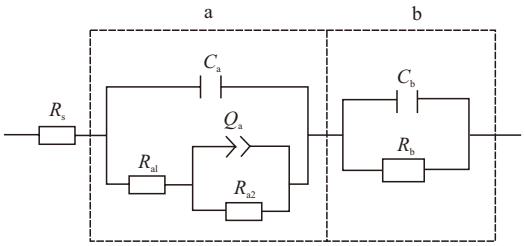

Fig.5 Equivalent circuit for EIS of AA7003 under various tempers

The electrical equivalent circuit is employed to model the spectra, as shown in Fig.5. The circuit of "a" denotes the IGC behavior between crystalline grains inside the alloy, the circuit of "b" stands for the reaction between the corrosion solution and the surface of aluminum matrix. R_s stands for the solution resistance, C_a and R_{a1} represent the electric double-layer capacitance and solution resistance of IGC crack inside the alloy respectively; Q_a and R_{a2} represent the constant phase angle element and reaction resistance of IGC inside alloy; C_b and R_b stand for the electric double-layer capacitance and polarization reaction resistance between the solution and the surface of matrix. The EIS fitting results of IGC are shown in Table 4. The value of reaction resistance (R_r) of the whole corrosion process is the summation of the R_a (R_{a1}+R_{a2}) and R_b, because all resistances of the electrical equivalent circuit are in series. In addition, the fitting results showed that the reaction resistance of the electrode reaction achieves the maximum value under the temper of RRA, the value of DPA is moderate, and that of PA is the least. This suggests that the extent of IGC follows the following order: RRA<DPA<PA, which is consistent with the results of the potentiodynamic polarization tests.

3.3 TEM observations

Fig.6 illustrates the TEM images of the AA7003 of PA, DPA, RRA tempers. A continuous feature of

Table 4 EIS fitting results of AA7003 tested in intergranular solution

Temper	R_s/(Ω·cm²)	C_a		R_{a1}/(Ω·cm²)	Q_a		R_{a2} /(Ω·cm²)	C_b /(F/cm²×10⁻⁶)	R_b /(Ω·cm²)
		Y_0/(Ω⁻¹·cm⁻²s⁻ⁿ×10⁻⁶)	n		Y_0/(Ω⁻¹·cm⁻²s⁻ⁿ×10⁻⁶)	n			
PA	4.743	13.721	0.112 4	5.895	14.43	0.780	3.794	941.5	12.3
DPA	5.370	18.482	0.593 6	5.419	29.03	0.828	5.604	1 096	22.4
RRA	4.467	16.200	1	2.808	29.37	0.536	8.056	1 298	29.1

grain boundary precipitates is shown in the image for the PA temper (Fig.6(a)). However, the AA7003 of DPA temper shows a discontinuous feature (Fig.6(b)) and the AA7003 of RRA temper displays wide precipitation free zones (PFZ) at grain boundary (Fig.6(c)). It is well known that the corrosion of Al-Zn-Mg-Cu aluminum alloys is closely related to the distribution of η precipitates on grain boundary, and η precipitates are identified as being anodic to the Al alloy matrix[26]. The IGC resistances of aluminum alloys are determined by the grain boundary microstructure, and the reason is that IGC usually initiates at grain boundaries. An active corrosion path will occur when η precipitates distribute continuously at grain boundaries (*e g*, PA), which is caused by the galvanic reaction between the anodic precipitates "η" at the grain boundaries and the peripheral alloy base.[27,28] Furthermore, the grain boundaries distributed with η precipitates will become an ideal segregation area of H, which results from the incoherent connection between η and periphery. Hence, the η precipitates will make aluminum alloys to have high susceptibility to corrosion and hydrogen embrittlement. However, the treatment of DPA and RRA changes the distribution of η precipitates on grain boundary, which decreases the susceptibility to corrosion and hydrogen embrittlement. In addition, compared with the other two tempers, AA7003 of RRA temper is of the highest IGC resistance because of the existence of wide PFZ at grain boundary.

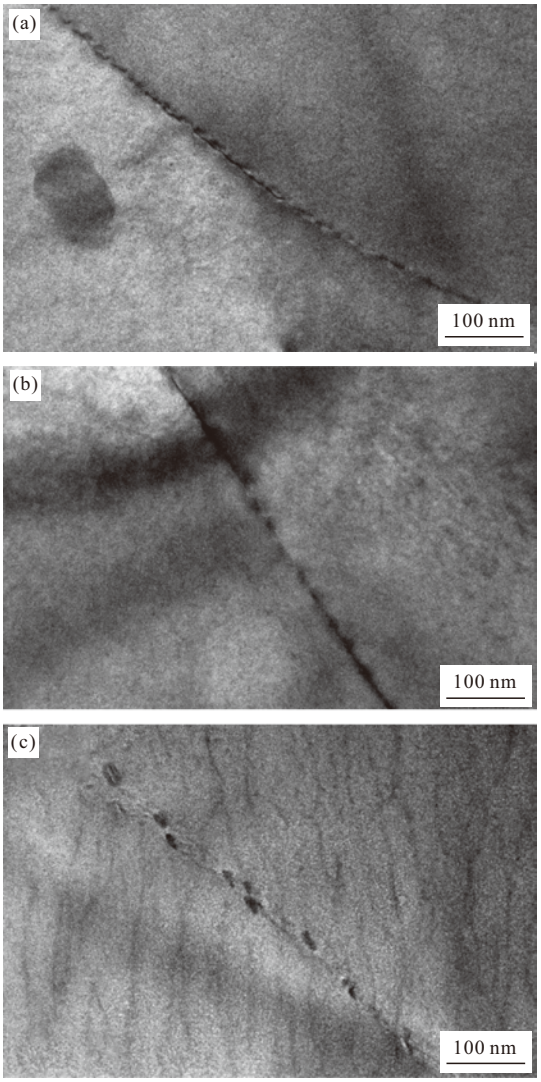

Fig.6 TEM images of AA7003 under various tempers: (a) PA; (b) DPA; (c) RRA

3.4 Slow strain rate test

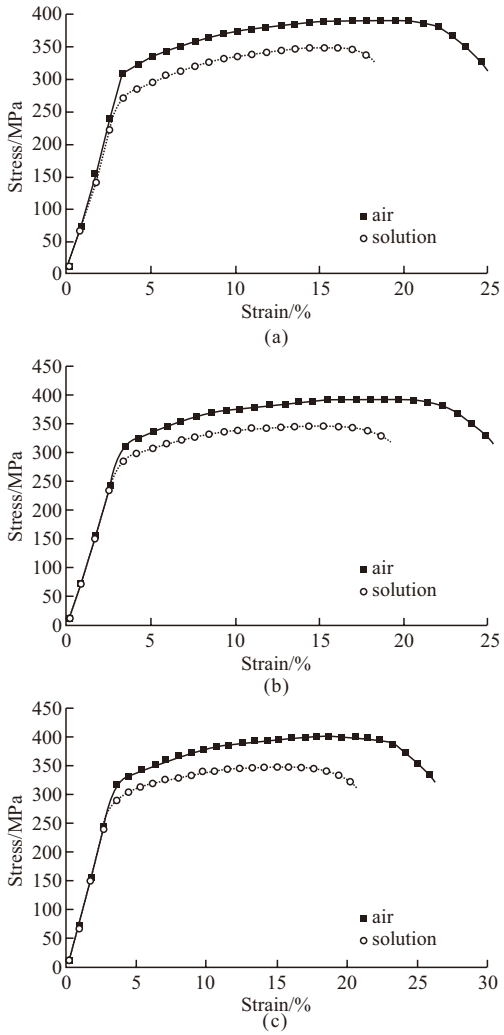

Fig.7 Stress-strain curves of AA7003 under various tempers in air and IGC solution: (a) PA; (b) DPA; (c) RRA

The stress-strain curves of AA7003 under various tempers measured in air and in IGC solution are shown in Fig.7. It is shown that both the elongation and mechanical strength of AA7003 under different aging treatments descend compared with that in air, indicating the occurrence of SCC under various tempers. Furthermore, the elongations of specimens

under various tempers are different, the PA temper achieves about 18.3%, the DPA temper has 19.2% and the RRA temper reaches approximately 19.9%. Thus, it is suggested that the aging treatment has great influence on the SCC behavior of AA7003.

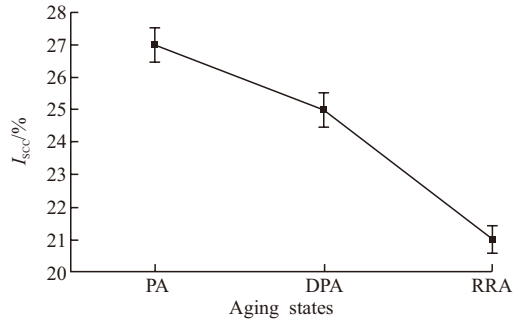

Fig.8 Dependence of SCC susceptibility on various tempers

In order to analyze the SCC behavior of AA7003 under various tempers in IGC solution, the SCC susceptibility (I_{SCC}) under various tempers was evaluated by the loss percentage of elongation. The dependence of I_{SCC} on tempers is shown in Fig.8. The I_{SCC} of AA7003-PA temper is higher than that of DPA temper and RRA temper, and the I_{SCC} of RRA temper is the least. The PA temper has the I_{SCC} of 27%, and that of DPA temper reduces to 25%, however, RRA reduces to 21% rapidly. The reason for this behavior is that the aging treatment affects the precipitation distribution. The grain boundary becomes short circuit diffusion channel and the preferential nucleation site because of the high interfacial energy. It is easy to form element segregation during solid solution treatment, and the solute atoms in the vicinity of the grain boundary are easy to diffuse to the grain boundary. Then continuous precipitation phase "η" ($MgZn_2$) precipitates preferentially at grain boundary, and η precipitates in Al-Zn-Mg-Cu alloy are more electrochemically active than the matrix. Hence, the grain boundaries with continuous η phase will become the susceptive anode channel, and the continuous η precipitates offer a path for SCC. The η precipitates preferentially dissolve in corrosion condition because of the galvanic action, act as crack initiation site, and consequently crack propagation occurs during the SSRT test, resulting in the highest I_{SCC} of PA. However, the precipitates of DPA are discrete, discontinuous, and widely distributed. These widely spaced and discontinuously distributed precipitates do not act as continuous network of corrosion path and channel for IGC, which results in an enhancement of resistance to SCC. Moreover, wider PFZ exists along the grain boundary in RRA, which decreases the dissolution in solution and reduces the tendency of IGC.

3.5 Fracture morphologies

The fractographs of AA7003 under various tempers tested in IGC solutions are shown in Figs.9(a)-9(f). It can be found from Figs.9(a), (b), (c) that obvious feature of dimples occurs when the samples are tested in air. Furthermore, the dimples of AA7003 of PA temper are shallower and larger than that of DPA and RRA temper, and a maximum number of dimples exist on the fracture morphology of alloy of RRA temper. Thus it is suggested that AA7003 of RRA temper has the greatest plasticity, DPA has the moderate plasticity and PA temper owns the least. However, characteristics of brittle intergranular rupture occurs as the AA7003 of the three tempers is tested in IGC solution, which indicates that IGC solution has a great influence on SCC behavior of AA7003. In addition, Fig.9(d) shows the characteristics of flat fracture and intergranular pores, while Fig.9(e) shows a mixure of intergranular fracture appearances and cleavage planes, and Fig.9(f) shows not only the feature of intergranular fracture, but also some quasi-cleavage surfaces and small dimples.

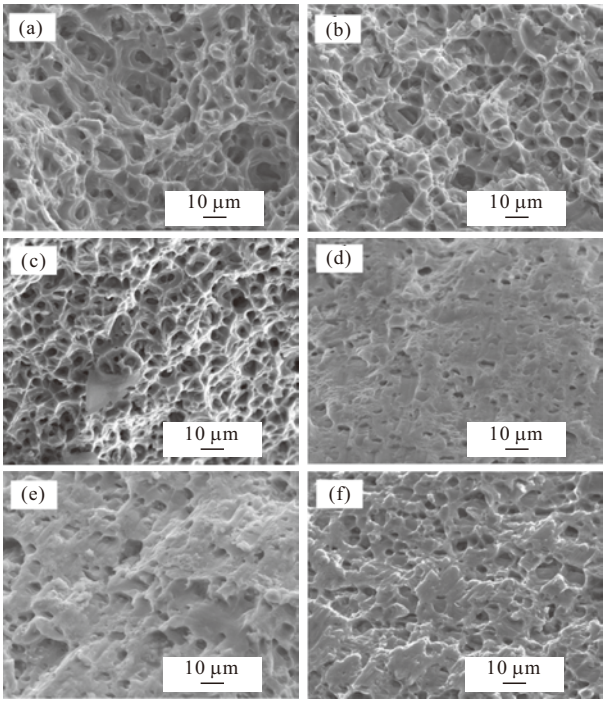

Fig.9 SEM fractographs of SSRT specimens of AA7003 in air and IGC solutions: (a) PA in air, (b) DPA in air, (c) RRA in air, (d) PA in solution, (e) DPA in solution, and (f)RRA in solution

On the basis of the analysis above, AA7003 under various tempers exhibits a certain extent of SCC susceptibility in IGC solution. Specifically, the

evolution of SCC of AA7003 with PA temper is faster and more active than that of AA7003 of DPA and RRA temper, which is consistent with the SCC susceptibility test results (Fig.8).

4 Conclusions

a) The IGC resistance of AA7003 under various tempers follows the order: PA<DPA<RRA, which is related to the precipitates distribution on the grain boundaries.

b) Compared with the continuous characteristics of precipitation phase η on grain boundary in AA7003 of PA temper, the DPA and RRA tempers exhibit the interrupted feature, and RRA temper is of wide PFZ.

c) AA7003 under various tempers exhibits a certain extent of SCC susceptibility in IGC solution, and I_{SCC} of PA is the highest, DPA moderate while RRA the lowest.

References

[1] Hill J A, Markley T, Forsyth M. Corrosion Inhibition of 7000 Series Aluminum Alloys with Cerium Diphenyl Phosphate[J]. *J. Alloy. Compd.,* 2011, 509(5): 1 683-1 690

[2] Xu D K, Birbilis N, Rometsch P A. Effect of S-Phase Dissolution on the Corrosion and Stress Corrosion Cracking of an As-Rolled Al-Zn-Mg-Cu Alloy[J]. *Corrosion,* 2012, 68(3): 1-10

[3] Huda Z, Edi P. Materials Selection in Design of Structures and Engines of Supersonic Aircrafts[J]. *Int. J. Mech. Mater. Des.*, 2013, 46(4): 552-560

[4] Dursun T, Soutis C. Recent Developments in Advanced Aircraft Aluminium Alloys[J]. *Mater. Design,* 2014, 56(4): 862-871

[5] Zhang X Y, Song R G, Sun B, *et al*. Effects of Applied Potentionals on Stress Corrosion Cracking Behavior of 7003 Aluminum Alloy in Acid and Alkaline Chloride Solutions[J]. *Int. J. Miner. Metall. Mater.*, 2016, 23(7): 819-826

[6] Qi X, Song R G, Qi W J, *et al*. Effects of Polarisation on Mechanical Properties and Stress Corrosion Cracking Susceptibility of 7050 Aluminum Alloy[J]. *Corros. Eng. Sci. Technol.,* 2014, 49(7): 643-650

[7] Rometsch P A, Zhang Y, Knight S. Heat Treatment of 7xxx Series Aluminium Alloys-Some Recent Developments[J]. *Trans. Nonferrous. Met. Soc. China*, 2014, 24(7): 2 003-2 017

[8] Mondal DP, Jha N, Badkul A. Effect of Al-TiB Master Alloy Addition on Microstructure, Wear and Compressive Deformation Behaviour of Aluminum Alloys[J]. *Trans. Nonferrous. Met. Soc. China*, 2012, 22(5): 1 001-1 011

[9] Marlaud T, Malki B, Henon C, *et al*. Relationship between Alloy Composition, Microstructure and Exfoliation Corrosion in Al-Zn-Mg-Cu Alloys[J]. *Corros. Sci.,* 2011, 53(10): 3 139-3 149

[10] Zupanc U, Grum J. Effect of Pitting Corrosion on Fatigue Performance of Shotpeened Aluminum Alloy 7075-T651[J]. *J. Mater. Process. Technol.,* 2010, 210(9): 1 197-1 202

[11] Rout P K, Ghosh M M, Ghosh K S. Influence of Aging Treatments on Alterations of Microstructural Features and Stress Corrosion Cracking Behavior of an Al-Zn-Mg Alloy[J]. *J. Mater. Eng. Perform.,* 2015, 24(7): 2 792-2 805

[12] Song R G, Dietzel W, Zhang B J, *et al*. Stress Corrosion Cracking and Hydrogen Embrittlement of an Al-Zn-Mg-Cu Alloy[J]. *Acta Mater.*, 2004, 52(16): 4 727-4 743

[13] Shi Y, Pan Q, Li M, *et al*. Influence of Alloyed Sc and Zr, and Heat Treatment on Microstructures and Stress Corrosion Cracking of Al-Zn-Mg-Cu Alloys[J]. *Mater. Sci. Eng. A*, 2015, 621: 173-181

[14] Qi X, Song R G, Qi W J, *et al*. Correspondence between Susceptibility to SCC of 7050 Aluminum Alloy and Passive Film Induced Stress at Various pH Values[J]. *J. Wuhan University of Technology-Mater. Sci. Ed.*, 2017, 32(1): 173-178

[15] Holroyd H, Scamans G M. Sensitization, Intergranular Corrosion, and Environment-Induced Cracking of Aluminum-Magnesium Alloys[J]. *Corrosion*, 2016, 72(2): 135-135

[16] Marlaud T, Deschamps A, Bley F, *et al*. Evolution of Precipitate Microstructures during the Retrogression and Re-ageing Heat Treatment of an Al-Zn-Mg-Cu alloy[J]. *Acta Mater.*, 2010, 58(14): 4 814-4 826

[17] Angappan M, Sampath V, Ashok B, *et al*. Retrogression and Reaging Treatment on Short Transverse Tensile Properties of 7010 Aluminum Alloy Extrusions[J]. *Int. J. Mech. Mater. Des.*, 2011, 32(7): 4 050-4 053

[18] Han N M, Zhang X M, Liu S D, *et al*. Effects of Pre-stretching and Ageing on the Strength and Fracture Toughness of Aluminum Alloy 7050[J]. *Mater. Sci. Eng. A,* 2011, 528(10-11): 3 714-3 721

[19] Xiao Y P, Pan Q L, Li W B, *et al*. Influence of Retrogression and Reaging Treatment on Corrosion Behavior of an Al-Zn-Mg-Cu alloy[J]. *Int. J. Mech. Mater. Des.*, 2011, 32(4): 2 149-2 156

[20] Wang Y L, Pan Q L, Wei L L, *et al*. Effect of Retrogression and Reaging Treatment on the Microstructure and Fatigue Crack Growth Behavior of 7050 Aluminum Alloy Thick Plate[J]. *Int. J. Mech. Mater. Des*., 2014, 55(6): 857-863

[21] Zheng C B, Yan B H, Zhang K, *et al*. Electrochemical Investigation of Hydrogen Permeation Behavior of 7075 T6 Al Alloy and Its Implication on Stress Corrosion Cracking[J]. *Int. J. Miner. Metall. Mater.*, 2015, 22(7): 729-737

[22] Qi X, Jin J R, Dai C L, *et al*. A Study on the Susceptibility to SCC of 7050 Aluminum Alloy by DCB Specimens[J]. *Materials*, 2016, 9(11): 884

[23] Nie X W, Zhang L J, Yong D U. Experiments and Modeling of Double-peak Precipitation Hardening and Strengthening Mechanisms in Al-Zn-Mg alloy[J]. *Trans. Nonferrous. Met. Soc. China*, 2014, 24(7): 2 138-2 144

[24] Shu W X, Hou L G, Zhang C, *et al*. Tailored Mg and Cu Contents Affecting the Microstructures and Mechanical Properties of High-strength Al-Zn-Mg-Cu Alloys[J]. *Mater. Sci. Eng. A,* 2016, 657: 269-283

[25] Li M H, Yang Y Q, Feng Z Q, *et al*. Precipitation Sequence of η Phase along Low-angle Grain Boundaries in Al-Zn-Mg-Cu Alloy during Artificial Aging[J]. *Trans. Nonferrous. Met. Soc. China*, 2014, 24(7): 2 061-2 066

[26] American Society for Testing and Materials. *Standard Practice for Evaluating Intergranular Corrosion Resistance of Heat Treatment Aluminum Alloys by Immersion in Sodium Chloride + Hydrogen Peroxide Solution*[S]. ASTM G110, 2009

[27] Song R G, Yang F E, Blawert C, *et al*. Behavior of Stress Corrosion Cracking in a Magnesium Alloy[J]. *J. Wuhan University of Technology-Mater. Sci. Ed.*, 2009, 24(1): 111-113

[28] Qi W J, Song R G, Zhang Y, *et al*. A Study on Mechanical Properties and Hydrogen Embrittlement Susceptibility of 7075 Aluminum Alloy[J]. *Corros. Eng. Sci. Technol.,* 2015, 50(6): 480-486